An Optoelectronic Resistive Switching Memory with Integrated Demodulating and Arithmetic Functions

Hongwei Tan, Gang Liu, Xiaojian Zhu, Huali Yang, Bin Chen, Xinxin Chen, Jie Shang, Wei D. Lu, Yihong Wu, and Run-Wei Li**

The integration of multiphotonic-functionalities, including the on-chip sources, manipulators, filters, multipliers, detectors, and storage, into microelectronic platforms, has been considered as an alternative solution for the size-scaling and intellectualization campaign of the post-Moore era.[1–6] An important module of such optoelectronic integrated circuits would be the field-induced resistive switching memory, the major task of which is to write and store the electrical bits of information through optical means.[7–13] Additional merits of the communication and computation capabilities may also lower the complexicity of the integrated circuits and make them more proficient when dealing with the rapidly increased massive data generated nowadays. Over the past few years, various semiconductor materials and nanostructures of silicon,[14] organic molecules,[15–18] carbon nanotubes,[19,20] graphene,[21,22] molybdenum disulfide and its analogs,[23–25] as well as metal oxides have been investigated for information storage and processing applications seperately.[26–28] Nevertheless, it is still challenging at the moment to achieve multifunction integration of efficient information storage, processing, and communication within a single device for the sake of high-performance optoelectronic circuits.

In this contribution, we report the design and construction of an optoelectronic resistive switching memory (OE-Memory) with integrated demodulating and arithmetic functions, composed of a simple ITO/CeO_{2-x}/AlO_y/Al junction structure (**Figure 1**a), for future information technology. Due to the detraping/retrapping of electrons within the interfacial CeO_{2-x} layer next to the AlO_y intercalation, which effectively modulates the band bending at the CeO_{2-x}/AlO_y/Al region, the intrinsic conductivity of the ITO/CeO_{2-x}/AlO_y/Al structure can be significantly modulated upon being subjected to optical illumination pulse and electrical stimulation pulse, thus leading to persistent and adjustable photoresponse in the present devices. The intensity- and wavelength-dependent resistances can be used to demodulate the broadband optical information into electrical signals, while the stepwise and linear response of the photocurrent makes the device capable of performing counting and addition operations. More importantly, the received optical digital signals can be stored non-volatilely by the multilevel and persistent photoresponses of the device, thus providing considerable potential for non-volatile optoelectronic memory devices with higher information storage and processing capacity.

To construct the ITO/CeO_{2-x}/AlO_y/Al junction (Figure 1b), a 30 nm thick Al electrode was first deposited by electron-beam evaporation on a commercial Si-based substrate. Then the polycrystalline CeO_{2-x} layer with the thickness of ≈20 nm has been deposited by magnetron-sputtering technique. Finally, the 100 µm-diameter ITO electrodes with the thickness of ≈200 nm were fabricated by pulsed laser deposition with good electrical conductivity and excellent optical transparency.[29] In this work, cerium oxide with a fluorite crystalline structure (Figure S1, Supporting Information) has been selected as the photo-sensitive medium for its semiconducting properties and tolerance of oxygen vacancy defects, which can provide extra defect energy levels in the bandgap to widen the wavelength window of the photoresponses.[30–33] By using aluminum as the bottom electrode, a native aluminum oxide layer with the thickness of ≈5 nm has been received to form the Schottky junction with the cerium oxide layer (Figure S2, Supporting Information), serving as an insulating barrier at the CeO_{2-x}/AlO_y/Al junction to suppress the leakage current and to enhance the signal-to-noise ratio of the devices.[34] The AlO_y/Al layer would also act as a reservoir to grab oxygen content during the CeO_{2-x} deposition process, therefore generating more oxygen vacancies in the cerium oxide film near the CeO_{2-x}/AlO_y/Al interface, as compared to that at the CeO_{2-x} film top surface (Figure S3, Supporting Information),[35,36] which provide stable interfacial trapping cites for the charge carriers.[37] Upon being exposed to an optical illumination, electrons in the trapping sites can be excited and swept away by the build-in electric field, leaving the positively charged oxygen vacancies to intensify the band bending at the CeO_{2-x}/AlO_y/Al interfacial region and facilitate the charge transport across the junction persistently with a thinner Schottky barrier (Figure 1c). When an external negative electrical-field is applied to the ITO/CeO_{2-x}/AlO_y/Al device,

H. Tan, Prof. G. Liu, Dr. X. Zhu, H. Yang, Dr. B. Chen, X. Chen, Dr. J. Shang, Prof. R.-W. Li
Key Laboratory of Magnetic Materials and Devices
Ningbo Institute of Materials Technology and Engineering
Chinese Academy of Sciences
Ningbo 315201, PR China
E-mail: liug@nimte.ac.cn; runweili@nimte.ac.cn

H. Tan, Prof. G. Liu, Dr. X. Zhu, H. Yang, Dr. B. Chen, X. Chen, Dr. J. Shang, Prof. R.-W. Li
Zhejiang Province Key Laboratory of Magnetic Materials and Application Technology
Ningbo Institute of Materials Technology and Engineering
Chinese Academy of Sciences
Ningbo 315201, PR China

Prof. W. D. Lu
Department of Electrical Engineering and Computer Science
University of Michigan
Ann Arbor, Michigan 48109, USA

Prof. Y. Wu
Information Storage Materials Laboratory
Department of Electrical and Computer Engineering
National University of Singapore
4 Engineering Drive 3, Singapore 117583, Singapore

DOI: 10.1002/adma.201500039

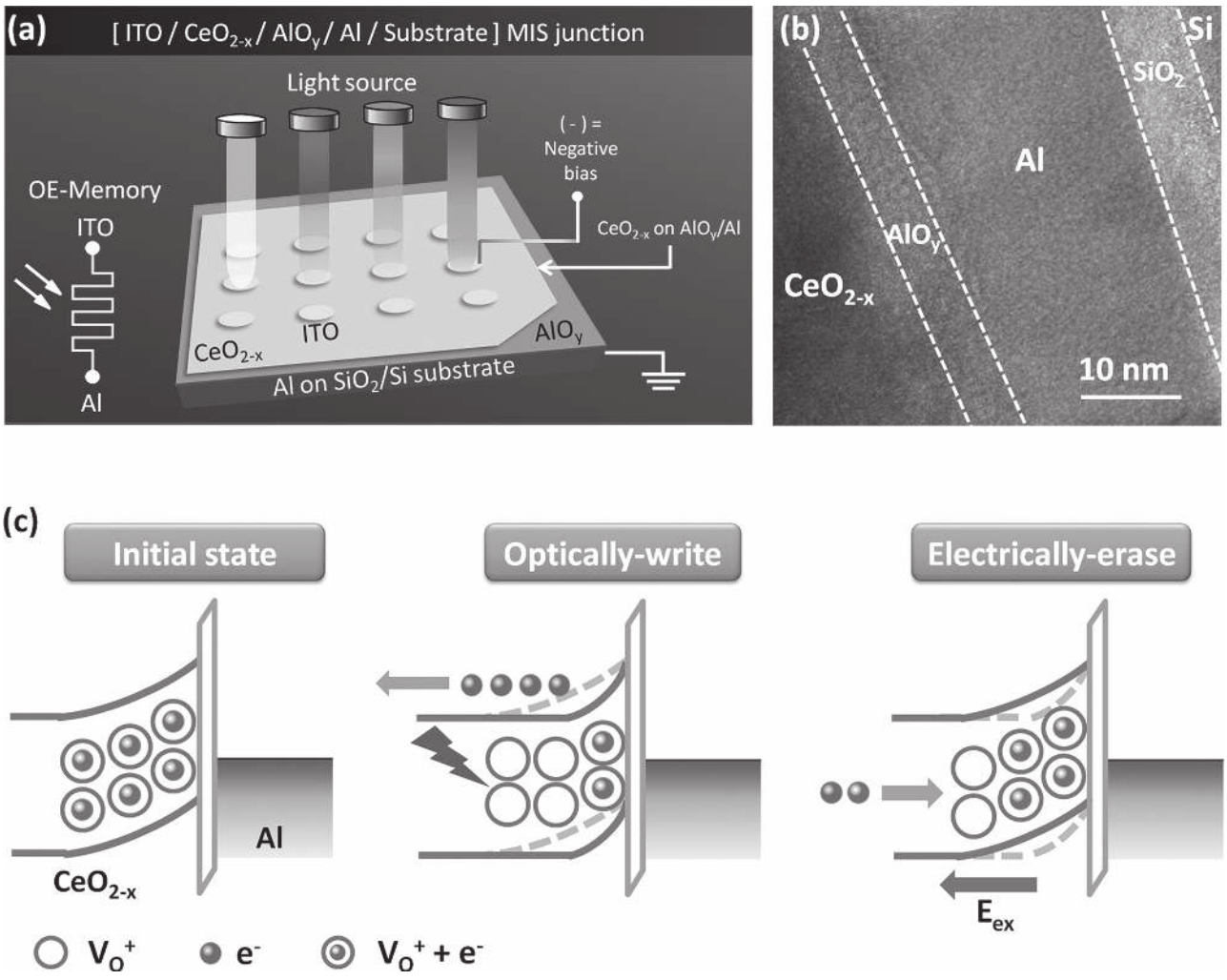

Figure 1. Device architecture and physical model for the electrically erasable persistent photoresponses. a) Schematic illustration of the ITO/CeO_{2-x}/AlO_y/Al junction structure and operation principle of the multifunctional optoelectronic resistive switching memory (OE-Memory). b) High-resolution transmission electron microscopic image of the CeO_{2-x}/AlO_y/Al junction deposited on SiO_2/Si substrate. c) Schematic illustration of the energy band diagram of CeO_{2-x}/AlO_y/Al MIS junction under optical illumination and electric field stimulations. The light-gray arrows illustrate the direction of electron transport while the dark-gray arrow shows the polarity of the applied electric field.

electrons will be injected into the interfacial trapping sites again and recover the initial energy band diagram.

Experimental data well agree with the above model. As shown in the current–voltage (*I*–*V*) characteristics of **Figure 2**a, electrically erasable persistent photoresponse has been observed in the present device. With the nominal bandgap of ≈3.3 eV for the CeO_2 thin films grown at room temperature,[38] an absorption cut-off wavelength of ≈375 nm should be theoretically expected. However, the introduction of oxygen vacancies and consequently the rich defect-energy levels in the bandgap, nevertheless, further extends the light absorption of the CeO_{2-x} layer from the ultraviolet into the visible region (Figure S4a, Supporting Information).[29–31] When the device is swept from 0 to +2 V and 0 to −2 V (Al bottom electrode was grounded and ITO was biased), an obvious rectification effect with the rectifying ratio of ≈10^4 (read at ±2 V) can be observed. This is in good agreement with the n-type semiconducting nature of cerium oxide and the present of defect levels in the bandgap for electron conduction, wherein the electrons will be injected into the defect levels in the bandgap instead of into the conduction bands. The device resistance is ≈3×10^{10} Ω at 0.1 V read voltage. Upon being exposed to the 400–800 nm broadband emission of the halogen lamp at 60 pW μm^{-2} for 20 s (Figure S4b , Supporting Information), the device can be programmed into a lower resistance (≈1×10^9 Ω) state with the ON/OFF ratio of ≈30. The photoresponsivity of the device is ≈1 A W^{-1} (read at 2 V), when the illumination duration is further increased to 100 s. The rectification effect is also reduced significantly. Nevertheless, the low resistance state can be well maintained after removing the optical illumination, indicating the persistent nature of the observed photoresponse in the ITO/CeO_{2-x}/AlO_y/Al device.

When a voltage pulse with the height of −2 V and the duration of 0.1 s has been applied onto the device, the multilayer structure can be programmed back to the initial high resistance state, with the initial rectifying properties also recovered. The

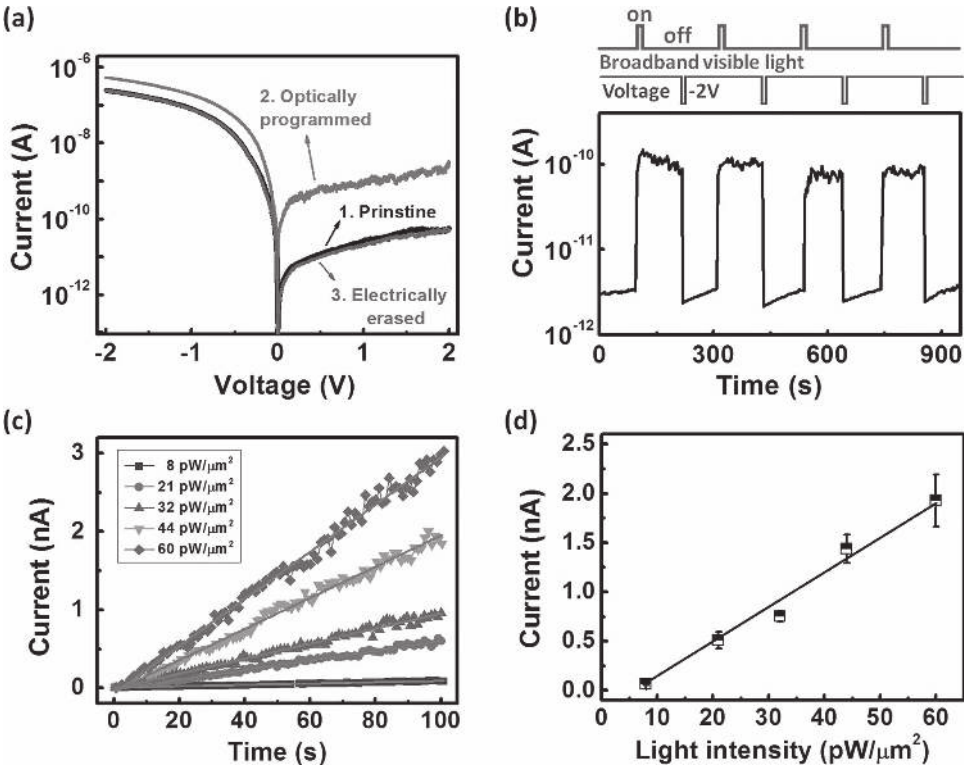

Figure 2. Photoresponse of the ITO/CeO_{2-x}/AlO_y/Al structure. a) Current–voltage characteristics of the device: (1) in dark, (2) after being exposed to 400–800 nm broadband illumination at 60 pW μm^{-2} for 20 s, as well as (3) after being subjected to a voltage pulse with the height of −2 V for 0.1 s. b) Reproducible photoresponse of the device after being alternatively exposed to broadband illumination with the intensity of 60 pW μm^{-2} for 20 s and voltage pulse with the height of −2 V for 0.1 s. c) Current–time characteristics of the ITO/CeO_{2-x}/AlO_y/Al multilayer structured device under broadband optical illumination with different intensities of 8, 13, 21, 32, 44, and 60 pW μm^{-2}, respectively. The symbols are the experimental results while the solid lines are fitted lines. d) Relationship between the photocurrent and the incident optical powers. The photocurrent was read at the illumination time of 100 s. In (b–d), the read voltage is 0.1 V.

optoelectronic switching of the device is reliable, where the alternative application of the light illumination and electrical stimuli can switch the ITO/CeO_{2-x}/AlO_y/Al structure between two resistance states with good reproducibility (Figure 2b). The present device also responds in the ultraviolet region, as well as exhibit electrically resistive switching behaviors (Figure S5 and S6, Supporting Information).[29] Since the photo-induced electron detrapping, electrode-injection, and retrapping processes of the ITO/CeO_{2-x}/AlO_y/Al structure, and consequently the band bending at the CeO_{2-x}/AlO_y/Al interfacial region, will be significantly influence by the history of the applied electric field, other resistance states would be reached when erasing voltage pulses with other magnitude and duration are used. Furthermore, as shown in Figure 2c,d, the linearity of the photocurrents in response to the incident light pulse width and intensity is in good agreement with the proposed model, wherein the accumulation effect of the photo-charged oxygen vacancies in the interfacial region will continuously modulate the photocurrent of the device (see Figure S7 and S8, Supporting Information for details). Thus, adjustable photoresponse has been demonstrated in the ITO/CeO_{2-x}/AlO_y/Al device, which can be used to achieve multiple information functions. On the other hand, the charging process will gradually slow down as the illumination continues, and the photocurrent will eventually stabilize at a saturated level.

Beyond the intensity-dependent photoresponsive resistances, the ITO/CeO_{2-x}/AlO_y/Al device also demonstrates broadband response to the light illumination over the entire visible region (**Figure 3**a). For instance, red illumination beam with the wavelength of 638 nm and a light power of 6 pW μm^{-2} (calibrated by the Li-250A Light Meter, Figure S4c, Supporting Information), which is obtained by passing the broadband emission through a commercial filter, can program the device to a resistance level of 2×10^{10} Ω. Similarly, the green and blue light beams with the same intensity of 6 pW μm^{-2} but different wavelengths of 560 and 499 nm, can set the device to much lower resistance levels of 8.5×10^9 and 1.6×10^9 Ω, respectively. All the three resistance states, together with the virgin state, can be optically programmed, maintained, electrically read and erased in cyclic operations (Figure 3b). Therefore, the present device is capable of converting the wavelength (or frequency) information of the incident light beam into electrical signals, as well as storing them simultaneously in the same device.

In the strategy of utilizing photons to communicate and using electrons to process the signals, one of the core components is the optoelectronic demodulator, which is used to convert the optical signals that carry information through their intensities and frequencies into electrical signals.[39,40] With both the intensity- and wavelength (frequency)-dependent persistent photoresponses of the ITO/CeO_{2-x}/AlO_y/Al structures,

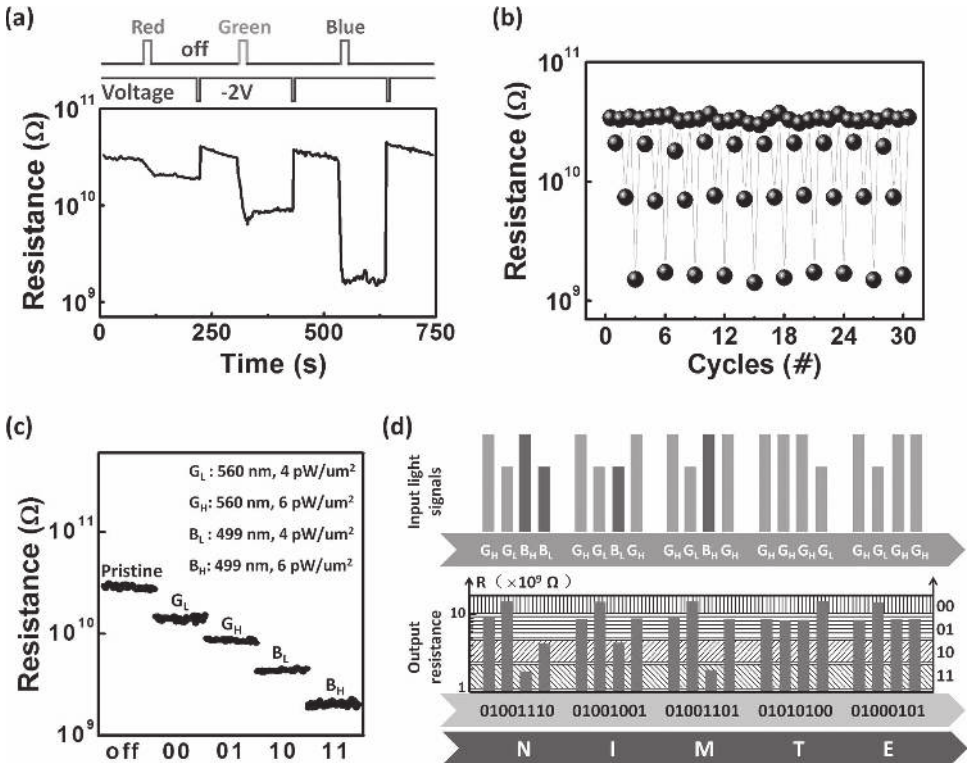

Figure 3. Optoelectronic demodulator and memory characteristics. a) Wavelength-dependent photoresponse and b) endurance performance of the device upon being exposed to the monochromic illumination with the wavelength of 638, 560, and 499 nm and identical intensities of 6 pW μm^{-2}, respectively. c) Decoding of the two-digit information of "00," "01," "10," and "11" with the light pluses with the wavelengths and intensities of 560 nm and 4 pW μm^{-2} (G_L), 560 nm and 6 pW μm^{-12} (G_H), 499 nm and 4 pW μm^{-2} (B_L), as well as 499 nm and 6 pW μm^{-2} (B_H), respectively. d) Demodulating of the word "NIMTE" according to eight-bit codes of the American Standard Code for Information Interchange.

an optical information demodulator has been demonstrated. Herein a two-digit piece of information, which is carried through the two degrees of freedom of a single light beam, namely the wavelength and intensity, can be accurately demodulated and stored by the resistance responses of the present device. For instance, the first-digit information can be transmitted with and demodulated from the wavelength of the light beam. The wavelengths of 560 nm for the green light and 499 nm for the blue light can be demodulated as "0" and "1," respectively. On the other hand, the second-digit binary information can be carried and demodulated with the intensity of the light beam, where 4 and 6 pW μm^{-2} for either colored light stand for "0" and "1," respectively. Thus, the four pieces of two-digit information of "00," "01," "10," and "11" can be demodulated and stored from the wavelength and intensity of the incident light beams, with the corresponding device resistances of $\approx 1.5 \times 10^{10}$, 9.0×10^{9}, 4.3×10^{9}, and 1.7×10^{9} Ω in response to the optical beams of green light with lower intensity (G_L), green light with higher intensity (G_H), blue light with lower intensity (B_L) and blue light with higher intensity (B_H), respectively (Figure 3c).

Illustratively, a bundle of four light pluses with the wavelengths and intensities of 560 nm and 6 pW μm^{-2}, 560 nm and 4 pW μm^{-2}, 499 nm and 6 pW μm^{-2}, as well as 499 nm and 4 pW μm^{-2}, respectively, can be demodulated into the single letter "N" and stored with the ITO/CeO_{2-x}/AlO_y/Al device, through the standard eight-bit codes of "01001110" according to the ASCII codes. In order to avoid the interference between the sequentially imposed light beams (accumulation effect in general) and to guarantee the precise demodulation of the optical signals, the device was erased with an electrical pulse after reading each light bit. With the two degrees of freedom of a single light beam to carry the digital information, which can be readily read and stored by the present optical demodulator and memory devices, the operation for both the optical-modulator and demodulator can be simplified as compared to those only capable of using one degree of freedom and larger numbers of light beams to transmit an eight-bit code.[41,42] The other letters of the alphabet can be demodulated similarly. Therefore, the word "NIMTE", which is short for the name of our institute (Ningbo Institute of Materials Technology and Engineering), can be demodulated from the light signals by and stored in the ITO/CeO_{2-x}/AlO_y/Al MIS structure (Figure 3d).

The relationship between the photocurrent and light pulse number was also investigated for the realization of computing functions. As shown, the dark current of the ITO/CeO_{2-x}/AlO_y/Al structure is ≈2.0 pA (**Figure 4**a). When multiple identical input light pulses with the intensity of 60 pW μm^{-2} and duration of 3 s have been applied onto the device, the output current (read at 0.1 V) increases from 2.6 to 78.6 pA linearly, in response to the total input light pulse number increasing from 1 to 20. The observed linear relationship between the current output and the number of the input light pulses can be expressed as:

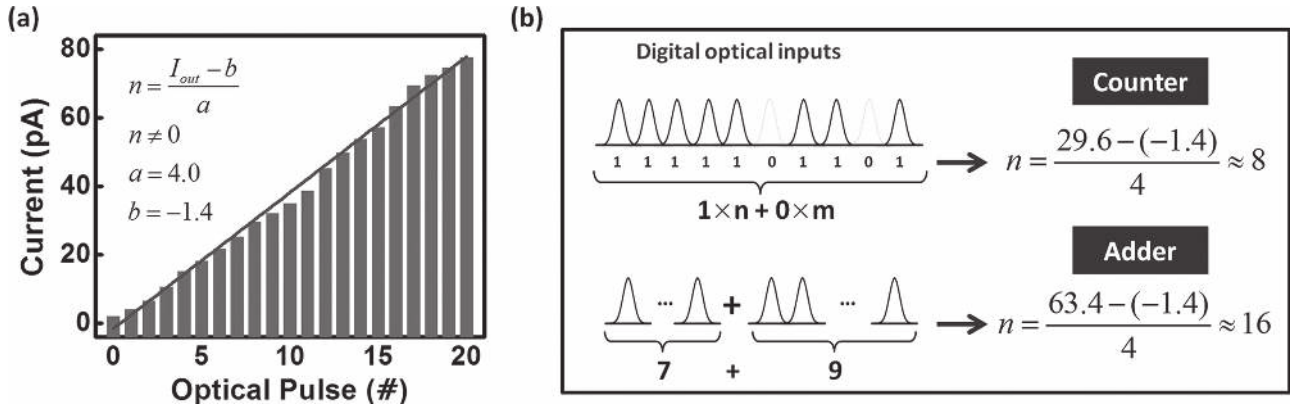

Figure 4. Optoelectronic arithmetic characteristics. a) Stepwise and linear relationship between the device output current and the number of the input light pulses. The solid line is fitted line. The read voltage is 0.1 V. I_{out}, n, a, and b stand for the output current (pA) of the device, number of the light pulse inputs, photocurrent ramping step of ≈4.0 (pA) per light illumination, and a constant of ≈−1.4 (pA), respectviely, for $n \neq 0$. The dark current is ≈2 pA for $n = 0$. b) Schematic illustration of the counting and adding operations that can be completed with the ITO/CeO_{2-x}/AlO_y/Al structure.

$$I_{out} = a \times n + b \quad (1)$$

$$n = \frac{I_{out} - b}{a} \quad (2)$$

where I_{out} is the output current (pA) of the device, n is the number of the light pulse inputs, a is the photocurrent ramping step of ≈4.0 (pA) per light illumination, and b is a constant of ≈−1.4 (pA), respectviely, for $n \neq 0$. The observed linear dependence of the device current on the total optical pulse numbers can be ascribed to the linear response of the photo-charged oxygen vacancies to the optical illuminations (see the Supporting Information for details). As such, the present "optical-input and electrical-output" device is capable of being operated as an arithmetic element for basic counting and adding operations. For instance, with the current readout of 29.6 pA for the optoelectronic arithmetic element, the total number of light pulses applied onto the device, 8 in this case, can be counted accordingly (upper panel of Figure 4b). Similarly, when a bundle of seven light pulses and a bundle of nine light pulses have been applied onto the arithmetic element sequentially, an output current of 63.4 pA, which equals to the photoresponse of a bundle of 16 light pulses, can be read from the optoelectronic device. Therefore, a simple adding operation of 7 + 9 = 16 can be completed with the ITO/CeO_{2-x}/AlO_y/Al structure (lower panel of Figure 4b). Nevertheless, the arithmetic operation is non-volatile and can be erased by negative voltage pulses, which makes the computing and memory functions achievable in a single device, thus allowing the design of scalable and complex computation architectures.[43,44]

The persistent nature of the photoresponse, nevertheless, allows the present device to function as a non-volatile resistive switching memory to electrically store the received optical information. In addition, the intensity-dependent photoresponsive resistances render the ITO/CeO_{2-x}/AlO_y/Al structure promising multilevel storage capabilities. For instance, when the device is exposed to the 400–800 nm broadband illumination of the halogen lamp with the lower intensities of 60, 21, and 8 pW μm^{-2} for 20 s, the device resistance can be programmed into levels of ≈1×10^9, 3×10^9, and 7×10^9 Ω, respectively (**Figure 5**a). Due to the accumulation effect as shown in Figure 2c, different illumination time can also be used to achieved multilevel storage. The device can be switched between the different resistances repeatedly, which shows the multilevel storage capability of an optoelectronic memory (Figure 5b). More importantly, the optically

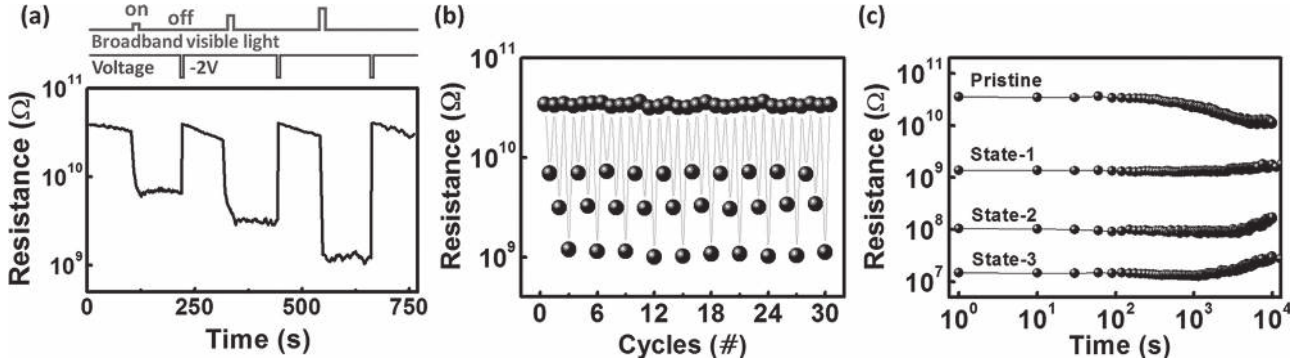

Figure 5. Non-volatile optoelectronic resistive switching memory characteristics. a) Intensity-dependent photoresponse of the device under broadband illumination with the intensities of 8, 21, and 60 pW μm^{-2}, respectively. b) Endurance performance of the device upon being exposed to optical illumination with different intensities as in (a). c) Retention performance of the resistance states programmed with the broadband illumination with different intensities for 100 s, respectively.

programmed resistance states remain distinguishable in air after 10^4 s upon removing the illumination source (Figure 5c), therefore allowing the non-volatile storage of the electrical information written by the optical means. Above all, the simple conceptual optoelectronic devices offer several advantages: i) For single-function application, these devices are capable of performing photodetection, optical information demodulation, multilevel information storage, and basic counting and adding tasks separately. ii) Some of the above functions, e.g., photodetection and demodulation, demodulation and memory, and arithmetic and memory, can be achieved simultaneously, which will lower the complexity and power consumption of the integrated circuit. iii) The introduction of both optical and electrical methods into integrated circuits will contribute to multifunctional optoelectronics and optoelectronic interconnection systems.

To summarize, due to the photo-induced electron detrapping, electrode-injection and retrapping processes of the ITO/CeO_{2-x}/AlO_y/Al structure, electrically erasable, multilevel and persistent photoresponsive resistances in the broadband visible region, which allow the integration of demodulating, arithmetic and memory functions in the same physical space, have been demonstrated in the present optoelectronic device. Though the challenge of slow speed, which hinders the optoelectronic device from immediate implementation, is still pending, the present finding demonstrates the possibility of using a photoresponsive device for future high-performance information storage, computing and communication applications.

Experimental Section

Characterization: The device structure and film thickness were determined using a JEOL 2100F transmission electron microscope (TEM) by SAE Magnetics (H.K.) Ltd. Company. The crystalline structure of the as-deposited CeO_{2-x} films was investigated by grazing-incidence X-ray diffraction technique (GIXRD) (Bruker AXS, D8 Discover) using Cu-K_α radiation. The incidence angle of X-ray beam was fixed at 1° and the measurements were recorded with a step of 0.04° in the range of 25–60°. The light absorption spectrum was recorded using UV–vis spectrometer (Perkin Elmer, Lambda 950) in the wavelength range from 300 to 800 nm. The spectra of broadband, red, green, and blue lights were measured using a fluorescence spectrometer (Hitachi F-4600) in the wavelength range from 350 to 750 nm. To confirm the existence of oxygen vacancies in the cerium oxide films, depth-profiling of cerium oxide films was performed using ion-etching treatment during X-Ray photoelectron spectroscopic (XPS) (Shimadzu, AXIS ULTRA DLD) measurements. A monochromatic Al-K_α X-ray source (1486.6 eV photons) was used at a constant dwell time of 100 ms. A pass energy of 80 or 40 eV was employed for the wide and core-level spectra scan, respectively. The X-ray source was run at a reduced power of 150 W (15 kV and 10 mA). The pressure in the analysis chamber was maintained at 10^{-8} Torr or lower during each measurement. The core-level signals were recorded at a photoelectron take-off angle (α, measured with respect to the sample surface) of 90°. All binding energies (BEs) were referenced to the C 1s hydrocarbon peak at 284.6 eV. A halogen lamp with broadband visible light was employed as the light source. Three commercial filters were used to produce the monochromic red, green and blue primary colored light beams. The intensities of light illuminations were characterized using a Li-250A Light Meter (LI-COR, Inc.). The photoresponsive current–voltage (I–V) characteristics of the ITO/CeO_{2-x}/AlO_y/Al structured devices were measured on a Lakeshore probe station equipped with a precision semiconductor parameter analyzer (Keithley 4200). To exclude the influence of environment lights, all the electrical measurements were conducted in the dark chamber of the Lakeshore probe station.

Supporting Information

Supporting Information is available from the Wiley Online Library or from the author.

Acknowledgements

The authors thank Prof. Shibing Long for the help of sample preparation for TEM measurements. The authors acknowledge the financial supports from the State Key Project of Fundamental Research of China (973 Program, 2012CB933004), National Natural Science Foundation of China (51303194, 61328402, 11474295, 11274322, and 61306152), the Instrument Developing Project of the Chinese Academy of Sciences (YZ201327), the Youth Innovation Promotion Association of the Chinese Academy of Sciences, Ningbo Major Project for Science and Technology (2014B11011), Ningbo Natural Science Foundations (2013A610031), and Ningbo International Cooperation Projects (2012D10018 and 2014D10005).
Note: Figure 1 was reset on May 4, 2015, after initial publication online.

Received: January 5, 2015
Revised: February 10, 2015
Published online: March 18, 2015

[1] V. R. Almeida, C. A. Barrios, R. R. Panepucci, M. Lipson, *Nature* **2004**, *431*, 1081.
[2] Y. A. Vlasov, X.-Z. Bo, J. C. Sturm, D. J. Norris, *Nature* **2001**, *414*, 289.
[3] Y. A. Vlasov, M. O'Boyle, H. F. Hamann, S. J. McNab, *Nature* **2005**, *438*, 65.
[4] L. Liu, R. Kumar, K. Huybrechts, T. Spuesens, G. Roelkens, E.-J. Geluk, T. D. Vries, P. Regreny, D. V. Thourhout, R. Baets, G. Morthier, *Nat. Photonics* **2010**, *4*, 182.
[5] H. Rong, R. Jones, A. Liu, O. Cohen, D. Hak, A. Fang, M. Paniccia, *Nature* **2005**, *433*, 725.
[6] J. Michel, J. Liu, L. C. Kimerling, *Nat. Photonics* **2010**, *4*, 527.
[7] R. Waser, M. Aono, *Nat. Mater.* **2007**, *6*, 833.
[8] J. Borghetti, G. S. Snider, P. J. Kuekes, J. J. Yang, D. R. Stewart, R. S. Williams, *Nature* **2010**, *464*, 873.
[9] S. H. Jo, T. Chang, I. Ebong, B. B. Bhadviya, P. Mazumader, W. Lu, *Nano Lett.* **2010**, *10*, 1297.
[10] M. Ungureanu, R. Zazpe, F. Golmar, P. Stoliar, R. Llopis, F. Casanova, L. E. Hueso, *Adv. Mater.* **2012**, *24*, 2496.
[11] J. Park, S. Lee, J. Lee, K. Yong, *Adv. Mater.* **2013**, *25*, 6423.
[12] A. Bera, H. Peng, J. Lourembam, Y. Shen, X. W. Sun, T. Wu, *Adv. Funct. Mater.* **2013**, *23*, 4977.
[13] C. Ye, Q. Peng, M. Li, J. Luo, Z. Tang, J. Pei, J. Chen, Z. Shuai, L. Jiang, Y. Song, *J. Am. Chem. Soc.* **2012**, *134*, 20053.
[14] C.-J. Kim, S.-J. Choi, J.-H. Ahn, J.-W. Han, H. Kim, S. Yoo, Y. K. Choi, *ACS Nano* **2012**, *6*, 1449.
[15] H. Dong, H. Zhu, Q. Meng, X. Gong, W. Hu, *Chem. Soc. Rev.* **2012**, *411*, 1754.
[16] Y. Yan, C. Zhang, J. Yao, Y. S. Zhao, *Adv. Mater.* **2013**, *25*, 3627.
[17] K. J. Baeg, M. Binda, D. Natali, M. Caironi, Y.-Y. Noh, *Adv. Mater.* **2013**, *25*, 4267.
[18] T. Iimori, N. Ohta, *J. Phys. Chem. C* **2014**, *118*, 7251.
[19] P. Avouris, J. Chen, *Mater. Today* **2006**, *9*, 46.
[20] Q. Cao, J. Rogers, *Adv. Mater.* **2009**, *21*, 29.

[21] C. Jia, H. Li, J. Jiang, J. Wang, H. Chen, D. Cao, J. F. Stoddart, X. Guo, *Adv. Mater.* **2013**, *25*, 6752.
[22] K. Roy, M. Padmanabhan, S. Goswami, T. P. Sai, G. Ramalingam, S. Raghavan, A. Ghosh, *Nat. Nanotechnol.* **2013**, *8*, 826.
[23] H. Wang, L. Yu, Y.-H. Lee, Y. Shi, A. Hsu, M. L. Chin, L.-J. Li, M. Dubey, J. Kong, T. Palacios, *Nano Lett.* **2012**, *12*, 4674.
[24] D.-S. Tsai, K.-K. Liu, D.-H. Lien, M.-L. Tsai, C.-F. Kang, C.-A. Lin, L.-J. Li, J.-H. He, *ACS Nano* **2013**, *5*, 3905.
[25] J.-K. Huang, J. Pu, C.-L. Hsu, M.-H. Chiu, Z.-Y. Juang, Y.-H. Chang, W.-H. Chang, Y. Iwasa, T. Takenobu, L.-J. Li, *ACS Nano* **2014**, *8*, 923.
[26] Y. Huang, C. M. Lieber, *Pure Appl. Chem.* **2004**, *76*, 2051.
[27] D. Panda, T.-Y. Tseng, *J. Mater. Sci.* **2013**, *48*, 6849.
[28] M.-P. Lu, M.-Y. Lu, L.-J. Chen, *Adv. Funct. Mater.* **2014**, *24*, 2967.
[29] J. Shang, G. Liu, H. Yang, X. Zhu, X. Chen, H. Tan, B. Hu, L. Pan, W. Xue, R.-W. Li, *Adv. Funct. Mater.* **2014**, *24*, 2171.
[30] C. B. Davis, D. D. Allred, A. Reyes- Mena, *Phys. Rev. B* **1993**, *47*, 13363.
[31] X. Z. Dang, C. D. Wang, E. T. Yu, K. S. Boutros, J. M. Redwing, *Appl. Phys. Lett.* **1998**, *72*, 2745.
[32] D. Nesheva, Z. Lev, Z. Aneva, V. Nikolova, H. Hofmeister, *J. Phys.: Condens. Matter* **2000**, *12*, 751.
[33] N. V. Skorodumova, S. I. Simak, B. I. Lundqvist, I. A. Abrikosov, B. Johansson, *Phys. Rev. Lett.* **2002**, *89*, 166601.
[34] X. Liu, L. Gu, Q. Zhang, J. Wu, Y. Long, Z. Fan, *Nat. Commun.* **2014**, *5*, 4007.
[35] A. Younis, D. Chu, S. Li, *J. Phys. D: Appl. Phys.* **2012**, *45*, 355101.
[36] E. J. Preisler, O. J. Marsh, R. A. Beach, T. C. McGill, *J. Vac. Sci. Technol. B* **2001**, *19*, 1611.
[37] E. Monroy, F. Calle, J. A. Garrido, P. Youinou, E. Munoz, F. Ommes, B. Beaumont, P. Gibart, *Semicond. Sci. Technol.* **1999**, *14*, 685.
[38] M. Mogensen, N. M. Sammes, G. A. Tompsett, *Solid State Ionics* **2000**, *129*, 63.
[39] G. Masini, S. Sahni, G. Capellini, J. Witzens, C. Gunn, *Adv. Opt. Technol.* **2008**, *2008*, 1.
[40] L. Chen, K. Preston, S. Manipatruni, M. Lipson, *Opt. Express* **2009**, *17*, 15248.
[41] J. Yoon, *Angew. Chem. Int. Ed.* **2014**, *53*, 6600.
[42] Y. Wu, Y. Xie, Q. Zhang, H. Tian, W. Zhu, A. D. Q. Li, *Angew. Chem. Int. Ed.* **2014**, *126*, 2122.
[43] Y. L. Kim, H. Y. Jung, S. Park, B. Li, F. Liu, J. Hao, Y.-K. Kwon, Y. J. Jung, S. Kar, *Nat. Photonics* **2014**, *8*, 239.
[44] H. Xu, Y. Xia, K. Yin, J. Lu, Q. Yin, J. Yin, L. Sun, Z. Liu, *Sci. Rep.* **2013**, *3*, 1230.